KSME

Springer

Journal of Mechanical Science and Technology 38 (4) 2024

Original Article
DOI 10.1007/s12206-024-0342-3

Keywords:
· Hydrophobic surface
· Hydrophilic surface
· Wettability transition
· Laser texturing

Correspondence to:
Jung Bin In
jbin@cau.ac.kr

Citation:
Ryu, C., Kim, H., Lee, H., In, J. B. (2024). Laser-induced selective wettability transition of 6061 aluminum alloy surfaces. Journal of Mechanical Science and Technology 38 (4) (2024) 2143~2150. http://doi.org/10.1007/s12206-024-0342-3

Received October 24th, 2023
Revised January 16th, 2024
Accepted January 17th, 2024

† Recommended by Editor Tong Seop Kim

Laser-induced selective wettability transition of 6061 aluminum alloy surfaces

Changyoung Ryu[1], Hakgae Kim[2], Hyoungsoon Lee[1,2] and Jung Bin In[1,2]

[1]School of Mechanical Engineering, Chung-Ang University, Seoul 06974, Korea, [2]Department of Intelligent Energy and Industry, Chung-Ang University, Seoul 06974, Korea

Abstract Laser texturing enables site-selective tailoring of wetting characteristics of metallic surfaces, converting the surfaces into hydrophilic or hydrophobic ones. In this study, selective wettability transition of 6061 aluminum alloy (Al 6061) surface is demonstrated by using a nanosecond fiber laser. The conversion of initial wettability of pristine Al 6061 into a near-superhydrophobic surface is achieved through laser irradiation of an Al 6061 plate and the following low-temperature thermal annealing. The wettability change is studied by measuring the water contact angle, and a significant increase in the angle (approximately, from 63.9° of pristine Al 6061 to 146.8°) is observed. Furthermore, the laser-textured hydrophobic surface is transformed into a hydrophilic surface by irradiating the surface again with the laser beam, resulting in superwetting ability. These wettability transitions are site-selectively obtained by exploiting the capability of direct laser writing, showcasing a promising potential in various applications.

1. Introduction

Surface wettability with water is an important characteristic of material surfaces, which stems from the interaction between liquid water molecules and material surfaces. Hydrophobic surfaces, characterized by a high contact angle with water droplets, possess the capability of repelling water, whereas hydrophilic surfaces promote water spreading and exhibit a low contact angle. The conversion of surface wettability from hydrophobic to hydrophilic surfaces, or vice versa, known as wettability transition, arises from modifications in surface energy. The wettability transitions provide a means of tailoring surfaces to achieve useful surface properties such as enhanced heat transfer [1-4], corrosion resistance [5], anti-icing [6, 7], and antibacterial surfaces [8], which can be applied in diverse advanced applications such as microfluidic devices [9], aircrafts [10], membranes [11], and biomaterials [12]. Surface roughness and chemical composition are known to critically determine the wettability [13, 14]. Various methods have been developed to modify these factors. For example, Ye et al. demonstrated superhydrophobicity of the silicon surface with nanocone arrays that were fabricated by chemical vapor deposition [15]. Zhuang et al. obtained a superhydrophobic Al1061 surface by modifying the surface morphology using a chemical etching method [16]. Li et al. fabricated a hydrophilic microchannel on a silicon wafer through deep reactive ion etching to enhance the flow boiling heat transfer [17].

Furthermore, the surface with heterogeneous wettability has been of interest to researchers because of its unique thermal properties. When the above-mentioned surface modifications are site-selectively achieved, both hydrophobic and hydrophilic properties can be imparted onto a single substrate surface. Many studies have reported extraordinary boiling heat transfer of these biphilic surfaces [18-21]. However, the fabrication of biphilic surface generally involves complicated micropatterning processes, such as photolithography or physical vapor deposition with a micropattern mask, typically resulting in increased production cost and extended processing time. Therefore, more facile fabrication approach is needed.

In this respect, laser surface texturing (LST) can be a promising solution to readily change the surface wettability by modifying the surface structure both physically and chemically. LST realizes maskless micropatterning on a surface owing to precise direct writing capability of focused laser beam scanning. Moreover, this method viably works even in ambient conditions because the oxygen and water in air help generate hydrophilic surface oxides [22]. In addition to the chemical modifications, the high-intensity focused laser beam promptly induces the ablation of the irradiated material, resulting in increased surface roughness [22-25]. As discussed above, this physical modification also contributes to the wettability change.

Researchers have developed various structures for wettability transition by LST on different metal substrates such as brass [26], copper [27], stainless steel [28], aluminum alloy [29], and titanium alloy [30]. While the laser irradiation of metal surface immediately induces the wettability change, long-term exposure to an ambient atmosphere is commonly observed to affect the surface wettability possibly due to the adsorption of airborne organic molecules to the activated surface, transforming the surface into a hydrophobic state [31]. Low-temperature annealing [31], hygrothermal treatment [32], and chemical coating [33] methods were developed to accelerate this transition in a controlled way. However, most of the existing laser methods for achieving biphilic metal surfaces have traditionally been assisted by coating with foreign chemicals, which involves additional chemical deposition processes [34, 35]. Accordingly, these methods suffer from the drawback of not only demanding extra processing time but also incurring additional costs. Therefore, it is necessary to explore a new method to address these drawbacks.

In this study, we demonstrate a facile fabrication of biphilic surfaces of 6061 aluminum alloy (Al 6061), which is widely known for its lightweight and good mechanical properties, by using nanosecond fiber lasers without assistance of additional chemicals. First, LST with the nanosecond laser produced a hydrophilic surface from a pristine Al 6061 surface. Subsequently, the hydrophilic surface was subject to low-temperature thermal annealing, which does not require additional chemical precursors for coating. The successfully treated Al 6061 sample exhibited ~146.8° of the water contact angle (WCA), showcasing near-superhydrophobicity. Finally, the obtained hydrophobic surface was irradiated with the laser again in a selected area, yielding a hydrophilic surface area again in the local area. This transition to hydrophilicity led to a superwetting surface that exhibited almost 0° of WCA, resulting in the coexistence of hydrophobic and hydrophilic areas on a single substrate.

2. Experimental

2.1 Materials and laser texturing

Fig. 1 shows the schematic of the biphilic (hydrophobic and hydrophilic) surface fabrication. A 3 mm thick Al 6061 plate was used as the base material. Prior to LST, the plate was polished using SiC sandpaper (P1200, P2400, and P4000, sequentially with careful cleaning between the steps) and the alumina suspensions (1 and 0.05 μm of particle sizes). This polishing procedure was necessary for removing the residual lubricant that is generally found on the surface of as-received Al plates. After the completion of the polishing sequences, the sample was immersed in ethanol and underwent deep cleaning in a bath sonicator to eliminate all the contaminants produced during the polishing process. For inducing hydrophilic surfaces, a nanosecond fiber laser (wavelength: 1062 nm, pulse duration: 250 nm, SPI Co.) was employed with a two-axis galvanometer scanner (DCB210-Y1HP, Thorlabs) coupled with an F-theta lens (focal length: 163 mm, Thorlabs). The diameter of the focused laser beam was estimated to be ~70.5 μm using the knife-edge method [36]. The laser processing parameters for 1st laser texturing are summarized in Table 1. The number of laser scanning (10) was specifically determined to achieve a maximum hydrophobicity, given the high scanning speed and laser power.

Table 1. 1st laser texturing conditions.

Laser power (W)/power density (kW/cm^2)	45/1150
Single pulse energy (mJ)/pulse fluence (J/cm^2)	0.9/23.1
Pulse frequency (kHz)	50
Scanning speed (mm/s)	500
Grid spacing (μm)	250
# of scanning repetition	10

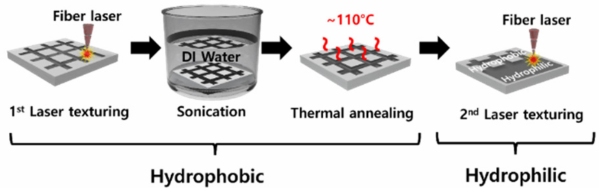

Fig. 1. Schematic illustrations for fabricating hydrophobic and hydrophilic surfaces.

The sample surface was irradiated with the laser beam that moved following a two-dimensional grid scanning path with a spacing of 0.25 mm. Thereafter, the sample was sonicated in DI water for 30 min for cleaning. The sample subsequently underwent a thermal annealing process in a convection oven at 110 °C for 12 h to promote the organic materials adsorption onto the surface [37]. This process not only accelerated the wettability transition but also yielded reliable results [31]. The 2nd laser texturing for selectively achieving hydrophilic surface was performed with the same processing parameters as those of the 1st laser texturing (Table 1) except for the laser power and grid spacing. For inducing hydrophilicity, the hydrophobic surface was raster-scanned with the nanosecond laser again (2nd laser irradiation), but the laser power was reduced to 30 W (pulse fluence: 15.4 J/cm^2). The line-to-line distance for raster scanning was 0.1 mm.

2.2 Wettability measurement

For measuring the wettability of sample surfaces, WCA with

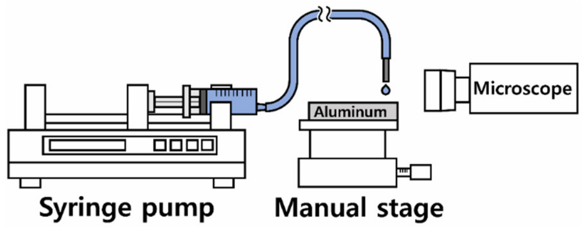

Fig. 2. Set up for contact angle measurement.

a water droplet was evaluated. For this measurement, deionized (DI) water was used, and the droplet volume was regulated to ~5 μl for minimizing the gravity effect (Bond number: ~0.156). This small volume was confirmed based on the droplet weight measured by a digital balance (AS 82/220.R.2, RADWAG). The WCA images were captured using an optical microscope (SCMOS-05000KPB, ASMETEC) in ambient conditions (relative humidity: 58 %, temperature: 23.9 °C). The measurement set up is presented in Fig. 2. WCAs were calculated by low bond axisymmetric drop shape analysis (LB-ADSA) of the imageJ software [38].

2.3 Material characterization

A field emission scanning electron microscope (FE-SEM, SIGMA, Carl Zeiss) was utilized to investigate the surface morphologies of the Al 6061 samples that underwent LST. To analyze the surface chemistry of the specimens, X-ray photoelectron spectroscopy (XPS, K-Alpha+, Thermo Fisher Scientific) was employed. XPS survey spectra were acquired using a pass energy of 200 eV with a step size of 1.0 eV, while the pass energy and step size were adjusted to 40 eV and 0.1 eV, respectively, for acquiring high-resolution spectra. Spectral shifts in the XPS data were corrected based on the reference peak position of C1s signals, which is placed at 284.8 eV. Surface topological images and height profiles were obtained using a laser confocal microscope (LEXT OLS 4100).

3. Results and discussion

3.1 Materials and laser texturing

The surface morphologies and high-resolution images of Al 6061 samples in each process are shown in Figs. 3(a)-(c). The LST surface area is approximately 10×10 mm^2. The peak intensity of laser at the center of the irradiated spot resembles the Gaussian-shaped distribution of the laser beam, leading to laser ablation primarily in the central region, with the intensity gradually decreasing in the surrounding area [39]. The ablation products ejected from the laser-irradiated area possess high kinetic energy resulting from the absorption of the intense laser beam and consequently disperse and deposit onto nearby areas [40]. While the inner square areas of the grid pattern were not directly irradiated with the laser, they were covered by irregularly shaped micro/nano-structures, suggesting rapid solidification of the ablation deposits. These structures can provide areas of air pockets, which trap air while interacting with liquid water, and consequently contribute to the hydrophobicity of the surface [28].

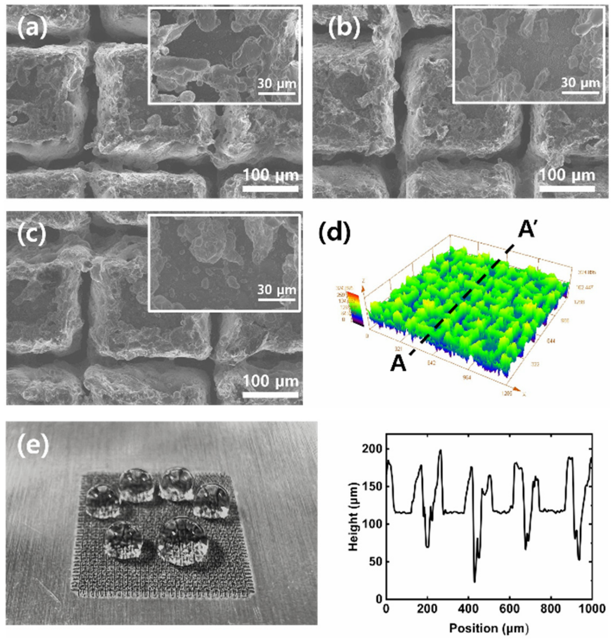

Fig. 3. Field-emission scanning electron microscopy top-view images of Al 6061 surface after: (a) 1st laser texturing; (b) sonication; (c) low-temperature thermal annealing. The insets show the corresponding high-resolution images; (d) topology image of the annealed surface and a cross-sectional height profile along the marked line (A–A'); (e) digital photography of hydrophobic Al 6061 surface and water droplets.

The SEM images (Figs. 3(a) and (b)) reveal that the surface morphologies of the laser-textured sample and the one cleaned in the bath sonicator are not considerably different, indicating a good adhesion between the ablation deposits and the underlying Al 6061 surfaces. The annealed sample did not exhibit apparent sintering of the small structures because of the low annealing temperature (Fig. 3(c)). Fig. 3(d) shows a topology image of the annealed surface. Its cross-sectional height profile along the marked line (A–A') reveals the heights of the ridges developed near the edges of laser ablation areas. The digital photography shown in Fig. 3(e) obviously displays the hydrophobicity of the thermally annealed Al 6061 surface.

While laser irradiation affects the surface structure in the laser texturing, excess heat generated in the Al 6061 plate can compromise structural integrity of the part, leading to irreversible deformation. However, structural deformation of the plate was not visually detected. The sample's bottom center temperature was measured using a thermocouple during the laser scanning, as depicted in Fig. 4(a) to approximately estimate the sample temperature. As shown in Fig. 4(b), the temperature only reached up to 55.4 °C, confirming the confinement of large heat near the surface and the moderate temperature increase far from the surface.

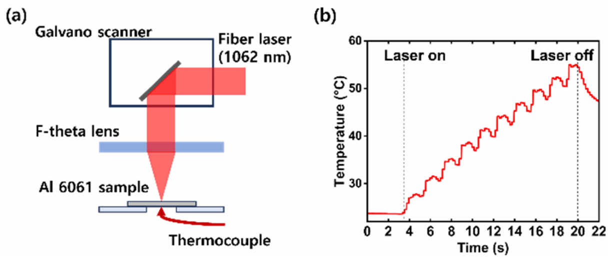

Fig. 4. (a) Schematic of temperature measurement; (b) temperature change measured at the bottom center of the Al 6061 sample during laser texturing.

3.2 Wettability change

There are three representative models (Young, Wenzel, and Cassie-Baxter models) used to explain the wettability behavior of surfaces. The Young's model serves as the simple method for understanding wetting behavior, and it results from the balance between the liquid-gas, solid-gas, and solid-liquid interfaces [41]. The wettability of a smooth and homogenous solid surface is determined by the surface free energy of the solid material. The simple contact angle (θ) was derived by Young's model, as shown Eq. (1).

$$cos(\theta) = \frac{\gamma_{sv} - \gamma_{sl}}{\gamma_{lv}} \quad (1)$$

where γ is the surface interfacial tension and the subscripts, *sv*, *lv* and *sl,* indicate solid-vapor, liquid-vapor, and solid-liquid interfaces, respectively. The Wenzel and Cassie-Baxter models are applied to understand the wettability properties on complex structure's surfaces. The Wenzel model is employed when the liquid completely permeates the rough surface of the solid, which have a larger surface area compared to smooth ones [42]. The apparent contact angle of Wenzel's model was proposed as Eq. (2).

$$cos(\theta *) = r\ cos(\theta) \quad (2)$$

where r denotes the solid surface roughness ratio of the wet solid surface. The Cassie-Baxter model is applicable when air becomes trapped in the grooves beneath the liquid, preventing the liquid from infiltrating into these structures [43]. The contact angle, as modified by Cassie-Baxter's model, can be described by Eq. (3).

$$cos(\theta **) = r f\ cos(\theta) + f - 1 \quad (3)$$

where f is the solid fraction and $(1 - f)$ is the vapor fraction.

Fig. 5 shows digital photography images of water contact to pristine, as-laser-textured, and annealed Al 6061 surfaces. WCA to these surfaces were approximately 63.9°, 0°, and 146.8°, respectively. The pristine Al 6061 exhibited a hydro-

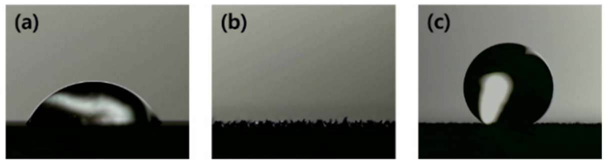

Fig. 5. Comparison of the water contact angle with (a) pristine; (b) as-laser-textured; (c) annealed Al 6061 surfaces.

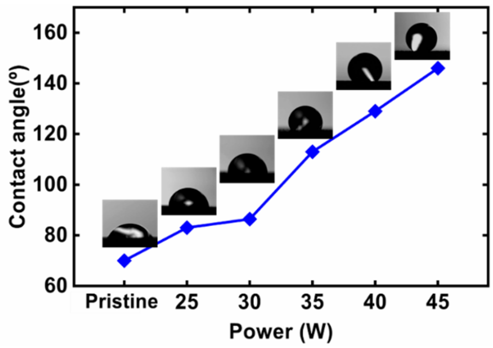

Fig. 6. Schematic illustrations for fabricating hydrophobic and hydrophilic surfaces.

philic surface (under 90°). For the as-laser-textured sample, the droplet quickly spread to the textured pattern area. The Al surface produced by laser-texturing followed by low-temperature annealing exhibited a large WCA close to superhydrophobicity (~150°). The wetting behavior of surface was further investigated by varying laser power from 25 to 45 W. Fig. 6 displays the resulting change in WCA with the increase in laser power. According to the Wenzel model, higher laser power resulted in an elevation of surface roughness, consequently resulting in an increased contact angle [44]. The surface became hydrophobic (WCA: 113°) at 35 W, which coincides with the threshold for laser ablation of Al 6061. Laser texturing created a valley structure that can form an air pocket, resulting in a wetting state where the Cassie-Baxter state prevails over the Wenzel state [45].

The surface chemistries of the Al 6061 surfaces were compared using XPS to identify the critical change in chemical elements by LST (Figs. 7 and 8). Fig. 7(a) shows the XPS survey spectrum of the pristine Al 6061 surface, which corresponds to the initially polished surface in this study, and Figs. 7(b) and (c) show the high-resolution Al2p and O1s spectra, respectively. The Al 2p peak is composed of the signal of Al metal (72.6 eV) and that of Al oxide (74.6 eV), which is formed by the adsorption of H_2O molecules in atmosphere [46]. The O 1s spectrum reveals two primary peaks associated with Al oxide (532.8 eV) and Al hydroxide (531.3 eV).

Likewise, Figs. 7(d)-(f) show the corresponding XPS survey, high-resolution Al2p, and O1s spectra, respectively, for the hydrophobic Al 6061 surface that was obtained after the low-temperature thermal annealing treatment. The XPS survey result reveals that the kinds of the surface elements remained almost unchanged after the laser texturing and the subsequent

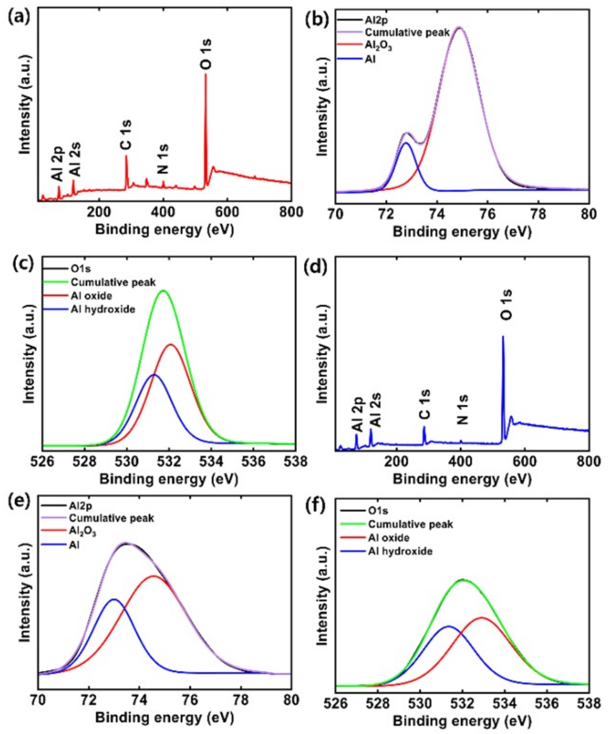

Fig. 7. (a) X-ray photoelectron spectroscopy (XPS) survey scan spectrum; (b) high-resolution Al2p spectrum; (c) high-resolution O1s spectrum of pristine Al 6061; (d) XPS survey scan spectrum; (e) high-resolution Al2p spectrum; (f) high-resolution O1s spectrum of hydrophobic Al 6061.

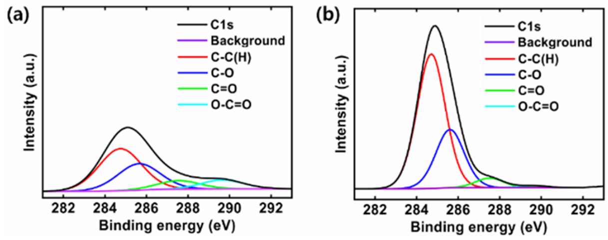

Fig. 8. High-resolution X-ray photoelectron spectroscopy C1s spectra of (a) as-laser-textured Al 6061 surface; (b) annealed surface.

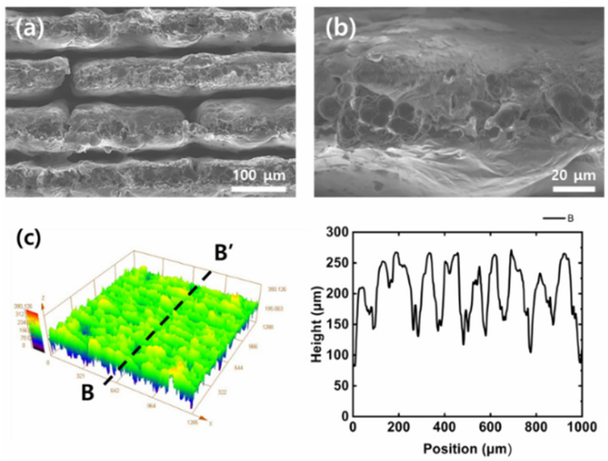

Fig. 9. (a) Top-view field emission scanning electron microscopy (FE-SEM) image of 2nd textured Al 6061; (b) top-view FE-SEM image of the 2nd textured Al 6061 captured at a high magnification; (c) topology image of the hydrophilic surface of 2nd textured Al 6061 and a cross-sectional height profile along the marked line (B–B').

thermal treatment. However, as shown in Fig. 7(e), for the hydrophobic surface, the intensity of Al metal was increased compared to that of Al oxide, indicating a reduced coverage of hydrophilic surface alumina. In addition, the concentration of aluminum hydroxide was increased from 38.8 % of the pristine surface to 43.15 % (Fig. 7(f)). Unsaturated Al^{3+} and O^- sites are known to be generated during the rapid passivation of the laser-ablated surface, and these active sites induce the hydroxylation reaction with airborne water molecules, producing the surface Al hydroxides [47, 48]. Brand et al. suggested that the Al hydroxides promote chemisorption of airborne carboxylates, eventually resulting in surface hydrophobicity [49]. While the annealing process accelerates this chemisorption [31], in our study, it also helped obtain reproducible WCA results. However, despite higher hydrophobicity of the annealed sample, the pristine Al surface exhibited a higher carbon content than the annealed sample (Figs. 7(a) and (d)). We believe that this is because the geometrical structure of the rough surface also significantly contributes to the hydrophobicity as discussed above.

For further investigating the influence of annealing on the surface chemistry, high-resolution C1s peaks of as-laser-textured and thermally annealed samples were obtained by XPS and compared (Fig. 8); notably, the C1s peak intensity of the annealed sample is obviously higher than that of the as-laser-textured sample, indicating increased carbon accumulation on the laser-textured surface by annealing. The C1s peaks were deconvoluted into four characteristic peaks of C-C(H), C-O, C = O, and O-C = O (284.7, 285.6, 287.5, and 289.6 eV, respectively). Herein, the functional group of C-C(H), which could derive from carboxylates in air moisture, is regarded as nonpolar and contributing to hydrophobicity [50]. The annealed surface exhibits a higher portion of this surface group (65.74 % in the C1s spectrum) than the as-laser-textured sample (48.89 %), which is consistent with its hydrophobic characteristic.

3.3 Wettability transition

After the 2nd laser irradiation for transition from hydrophobic to hydrophilic surfaces, the surface morphology was noticeably changed. Fig. 9 shows the top-view SEM images for this sample. Notably, evidence of significant surface melting was observed; the vertical valleys engraved by the 1st laser texturing were merged to a large structure with blunt edges (Fig. 9(a)). As shown in Fig. 9(b), previous microstructures observed on the top surface were enlarged possibly by melting and significant sintering. Fig. 9(c) shows a topology image of the surface and its cross-sectional height profile. It confirms the formation of blunt structures at the top surface, compared with Fig. 3(d). Consequently, this surface exhibited a through transition from

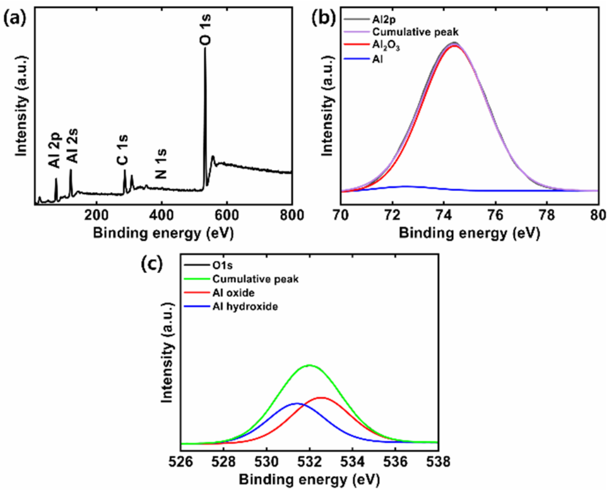

Fig. 10. X-ray photoelectron spectroscopy survey scan spectra of (a) hydrophilic Al 6061. High-resolution: (b) Al2p; (c) O1s in hydrophilic Al 6061.

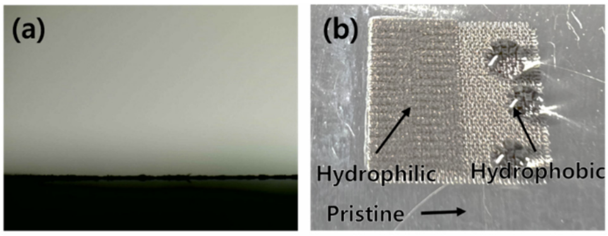

Fig. 11. (a) The water constant contact angle of 2nd laser-textured Al 6061; (b) digital image of hydrophilic and hydrophobic (biphilic) Al 6061.

hydrophobicity to hydrophilicity, confirming successful engineering of wettability.

XPS analysis was performed again to investigate the chemical composition of the hydrophilic surface. Fig. 10(a) presents the overall survey data peaks of the hydrophilic Al 6061. Fig 10(b) shows the sample's high-resolution XPS spectrum for Al 2p. The result clearly reveals a significant reduction of metallic Al peak signals and instead the dominating portion of hydrophilic surface alumina. The Al oxide (54.5 % in O1s spectrum) and Al hydroxide (45.5 %) concentrations, as shown in Fig. 10(c), remained almost the same as those of the hydrophobic Al 6061 surface (Fig. 5(f)). However, a marked decrease in C-to-Al atomic ratio is observed from the XPS data. For this hydrophilic Al 6061, the ratio is calculated to be ~0.66, whereas the ratio for the hydrophobic surface (annealed one) is ~0.88, suggesting the removal of surface carbon species by the 2nd laser irradiation.

The WCA of the Al 6061 surface, which underwent the second laser texturing, exhibited a WCA of nearly 0°, confirming the surface hydrophilicity (Fig. 11(a)). While this sample displays a bidirectional morphology (Fig. 9(a)), its bidirectional characteristics in WCA were not observed. This superwetting characteristic can be site-selectively imparted to a specific area of the hydrophobic surface by programming the laser scanning path. For instance, a biphilic surface can be prepared based on this method, and the characteristic surface geometry can be easily written by laser scanning. Fig. 11(b) depicts a digital photography of a Al6061 sample that was prepared based on the method developed in this study. The surface exhibits three distinct regions of different surface wettabilities: smooth pristine, hydrophilic (left), and hydrophobic areas (right).

4. Conclusions

In this study, hydrophobic and hydrophilic Al 6061 surfaces were obtained by LST. With a noteworthy difference from prior research, our investigation involved the retransition of surfaces that had already underwent wettability modification through the laser processing on the same substrate, showcasing biphilic properties. Despite possible drawbacks such as increased surface hardness and roughness, the processes are readily achieved with simple and fast laser scanning procedures, which are beneficial for selective and flexible property alternations of surface. Although the first laser-textured sample initially exhibited hydrophilic properties; its wettability was markedly changed by low-temperature thermal annealing. However, organic materials possibly adsorbed by this process were readily eliminated by the second irradiation with the laser, resulting in a reconversion of the surface from hydrophobic to hydrophilic one. The relationship between LST and wettability change was elucidated by SEM and XPS investigations. The laser-induced structure change resulted in roughness increases and the formation of air pocket sites on the surface, contributing to the alteration of wettability. These research findings are expected to provide valuable insights for the development of future surface treatment technologies to realize biphilic metal surfaces that can be applied in high-performance pool boiling surfaces.

Acknowledgments

This research was supported by the Challengeable Future Defense Technology Research and Development Program through the Agency for Defense Development (ADD) funded by the Defense Acquisition Program Administration (DAPA) in 2022 (No.915028201).

References

[1] Q. Zhao, J. Qiu, J. Zhou, M. Lu, Q. Li and X. Chen, Visualization study of flow boiling characteristics in open microchannels with different wettability, *International Journal of Heat and Mass Transfer*, 180 (2021) 121808.

[2] K. Vontas, M. Andredaki, A. Georgoulas, N. Miché and M. Marengo, The effect of surface wettability on flow boiling characteristics within microchannels, *International Journal of Heat and Mass Transfer*, 172 (2021) 121133.

[3] Y. Sun, Y. Tang, S. Zhang, W. Yuan and H. Tang, A review on fabrication and pool boiling enhancement of three-dimensional complex structures, *Renewable and Sustainable Energy Re-*

views, 162 (2022) 112437.

[4] P. Sen, S. Kalita, D. Sen, A. K. Das and B. B. Saha, Pool boiling heat transfer and bubble dynamics of modified copper micro-structured surfaces, *International Communications in Heat and Mass Transfer*, 134 (2022) 106039.

[5] D. Wei, J. Wang, S. Li, Y. Liu, D. Wang and H. Wang, Novel corrosion-resistant behavior and mechanism of a biomimetic surface with switchable wettability on Mg alloy, *Chemical Engineering Journal*, 425 (2021) 130450.

[6] A. Gaddam, H. Sharma, T. Karkantonis and S. Dimov, Anti-icing properties of femtosecond laser-induced nano and multiscale topographies, *Applied Surface Science*, 552 (2021) 149443.

[7] X. Li, G. Wang, A. S. Moita, C. Zhang, S. Wang and Y. Liu, Fabrication of bio-inspired non-fluorinated superhydrophobic surfaces with anti-icing property and its wettability transformation analysis, *Applied Surface Science*, 505 (2020) 144386.

[8] M. Luna, O. Beltran, D. A. Encinas-Basurto, M. G. Ballesteros-Monrreal, A. Topete, N. Hassan, M. A. López-Mata, V. Reyes-Márquez, M. A. Valdez and J. Juarez, High antibacterial performance of hydrophobic chitosan-based nanoparticles loaded with Carvacrol, *Colloids and Surfaces B: Biointerfaces*, 209 (2022) 112191.

[9] M. J. Männel, N. Weigel, N. Hauck, T. Heida and J. Thiele, Combining hydrophilic and hydrophobic materials in 3D printing for fabricating microfluidic devices with spatial wettability, *Advanced Materials Technologies*, 6 (9) (2021) 2100094.

[10] D. Zeng, Y. Li, D. Huan, H. Liu, H. Luo, Y. Cui, C. Zhu and J. Wang, Robust epoxy-modified superhydrophobic coating for aircraft anti-icing systems, *Colloids and Surfaces A: Physicochemical and Engineering Aspects*, 628 (2021) 127377.

[11] S. K. Hubadillah, Z. S. Tai, M. H. D. Othman, Z. Harun, M. R. Jamalludin, M. A. Rahman, J. Jaafar and A. F. Ismail, Hydrophobic ceramic membrane for membrane distillation: A mini review on preparation, characterization, and applications, *Separation and Purification Technology*, 217 (2019) 71-84.

[12] R. M. Visalakshan, M. N. MacGregor, S. Sasidharan, A. Ghazaryan, A. M. Mierczynska-Vasilev, S. Morsbach, V. Mailänder, K. Landfester, J. D. Hayball and K. Vasilev, Biomaterial surface hydrophobicity-mediated serum protein adsorption and immune responses, *ACS Applied Materials & Interfaces*, 11 (31) (2019) 27615-27623.

[13] W.-L. Zhou, T. Wu, Y. Du, X.-H. Zhang, X.-C. Chen, J.-B. Li, H. Xie and J.-P. Qu, Efficient fabrication of desert beetle-inspired micro/nano-structures on polypropylene/graphene surface with hybrid wettability, chemical tolerance, and passive anti-icing for quantitative fog harvesting, *Chemical Engineering Journal*, 453 (2023) 139784.

[14] D. Parbat, S. Gaffar, A. M. Rather, A. Gupta and U. Manna, A general and facile chemical avenue for the controlled and extreme regulation of water wettability in air and oil wettability under water, *Chem Sci*, 8 (9) (2017) 6542-6554.

[15] X. Huang, M. Sun, X. Shi, J. Shao, M. Jin, W. Liu, R. Zhang, S. Huang and Y. Ye, Chemical vapor deposition of transparent superhydrophobic anti-Icing coatings with tailored polymer nanoarray architecture, *Chemical Engineering Journal*, 454 (2023) 139981.

[16] R. Liao, Z. Zuo, C. Guo, Y. Yuan and A. Zhuang, Fabrication of superhydrophobic surface on aluminum by continuous chemical etching and its anti-icing property, *Applied Surface Science*, 317 (2014) 701-709.

[17] K. Luo, W. Li, J. Ma, W. Chang, G. Huang and C. Li, Silicon microchannels flow boiling enhanced via microporous decorated sidewalls, *International Journal of Heat and Mass Transfer*, 191 (2022) 122817.

[18] A. R. Betz, J. Xu, H. Qiu and D. Attinger, Do surfaces with mixed hydrophilic and hydrophobic areas enhance pool boiling?, *Applied Physics Letters*, 97 (14) (2010) 141909.

[19] Y. Xia, R. Li, X. Gao and R. Li, Pool boiling on a biphilic surface where bubbles can move horizontally on the surface, *International Journal of Heat and Mass Transfer*, 215 (2023) 124540.

[20] V. Serdyukov, G. Patrin, I. Malakhov and A. Surtaev, Biphilic surface to improve and stabilize pool boiling in vacuum, *Applied Thermal Engineering*, 209 (2022) 118298.

[21] Y. Zhu, C. Y. Tso, T. C. Ho, M. K. H. Leung, S. Yao and H. H. Qiu, Heat transfer enhancement on tube surfaces with biphilic nanomorphology, *Applied Thermal Engineering*, 180 (2020) 115778.

[22] Q. Cao, Z. Wang, W. He and Y. Guan, Fabrication of super hydrophilic surface on alumina ceramic by ultrafast laser microprocessing, *Applied Surface Science*, 557 (2021) 149842.

[23] H. Wan, J. Min, B.E. Carlson, J. Lin and C. Sun, Spindle-shaped surface microstructure inspired by directional water collection biosystems to enhance interfacial wetting and bonding strength, *ACS Applied Materials & Interfaces*, 13 (11) (2021) 13760-13770.

[24] W. G. Jiru, M. R. Sankar and U. S. Dixit, Laser surface alloying of copper, manganese, and magnesium with pure aluminum substrate, *Journal of Materials Engineering and Performance*, 25 (3) (2016) 1172-1181.

[25] A. Wang, C. Fan, C. Xie, W. Huang and K. Cui, Laser cladding of iron- base alloy on al-si alloy and its relation to cracking at the interface, *Journal of Materials Engineering and Performance*, 5 (6) (1996) 775-783.

[26] H. Yan, M. R. B. Abdul Rashid, S. Y. Khew, F. Li and M. Hong, Wettability transition of laser textured brass surfaces inside different mediums, *Applied Surface Science*, 427 (2018) 369-375.

[27] Z. Cao, Z. Ouyang, Z. Liu, Y. Li, Y. Ouyang, J. Lin, X. Xie and J. Long, Effects of surface oxides and nanostructures on the spontaneous wettability transition of laser-textured copper surfaces, *Applied Surface Science*, 560 (2021) 150021.

[28] C.-V. Ngo and D.-M. Chun, Fast wettability transition from hydrophilic to superhydrophobic laser-textured stainless steel surfaces under low-temperature annealing, *Applied Surface Science*, 409 (2017) 232-240.

[29] M. Abeens, R. Muruganandhan and K. Thirumavalavan, Effect of low energy laser shock peening on plastic deformation, wettability and corrosion resistance of aluminum alloy 7075

T651, *Optik*, 219 (2020) 165045.

[30] P. Zhou, Y. Liu, Q. Chen, H. Li, R. Bian, W. Xu, Q. Yang and D. Liu, Femtosecond laser-induced hydrophobic surface of niti shape memory alloy and its blood compatibility, *Physica Status Solidi (A)*, 220 (11) (2023) 2200747.

[31] C.-V. Ngo and D.-M. Chun, Effect of heat treatment temperature on the wettability transition from hydrophilic to superhydrophobic on laser-ablated metallic surfaces, *Advanced Engineering Materials*, 20 (7) (2018) 1701086.

[32] H. L. Wan, S. S. Li, J. J. Li, T. Liu, J. P. Lin and J. Y. Min, Wettability transition of metallic surfaces from laser-generated superhydrophilicity to water-induced superhydrophobicity via a facile and eco-friendly strategy, *Materials & Design*, 226 (2023) 111691.

[33] D. Mullangi, S. Shalini, S. Nandi, B. Choksi and R. Vaidhyanathan, Super-hydrophobic covalent organic frameworks for chemical resistant coatings and hydrophobic paper and textile composites, *Journal of Materials Chemistry A*, 5 (18) (2017) 8376-8384.

[34] M. Moze, M. Zupancic and I. Golobic, Pattern geometry optimization on superbiphilic aluminum surfaces for enhanced pool boiling heat transfer, *Int. J. Heat Mass Transfer*, 161 (2020) 120265.

[35] M. Zupancic, M. Moze, P. Gregorcic, A. Sitar and I. Golobic, Evaluation of enhanced nucleate boiling performance through wall-temperature distributions on PDMS-silica coated and non-coated laser textured stainless steel surfaces, *Int. J. Heat Mass Transfer*, 111 (2017) 419-428.

[36] J. M. Khosrofian and B. A. Garetz, Measurement of a Gaussian laser beam diameter through the direct inversion of knife-edge data, *Appl. Opt.*, 22 (21) (1983) 3406-3410.

[37] D. Zhang, Y. Wan and G. Nagayama, Superhydrophobicity of thermally annealed aluminum surfaces and its effect on corrosion resistance, *Applied Physics Letters*, 123 (9) (2023) 091603.

[38] A. F. Stalder, T. Melchior, M. Müller, D. Sage, T. Blu and M. Unser, Low-bond axisymmetric drop shape analysis for surface tension and contact angle measurements of sessile drops, *Colloids and Surfaces A: Physicochemical and Engineering Aspects*, 364 (1) (2010) 72-81.

[39] J. Alda, Laser and Gaussian beam propagation and transformation, *Encyclopedia of Optical Engineering*, Marcel Dekker, Inc, USA (2003) 999-1013.

[40] U. Nath and V. Yadav, Analytical modelling of 3D temperature evolution of Al 6061-T6 irradiated by a moving laser heat source considering intensive convective boundary conditions, *Journal of Mechanical Science and Technology*, 36 (12) (2022) 6247-6260.

[41] V. Bruce and A. Young, Understanding face recognition, *British Journal of Psychology*, 77 (3) (1986) 305-327.

[42] R. N. Wenzel, Resistance of solid surfaces to wetting by water, *Industrial & Engineering Chemistry*, 28 (8) (1936) 988-994.

[43] A. B. D. Cassie and S. Baxter, Wettability of porous surfaces, *Transactions of the Faraday Society*, 40 (1944) 546-551.

[44] V. D. Ta, A. Dunn, T. J. Wasley, J. Li, R. W. Kay, J. Stringer, P. J. Smith, E. Esenturk, C. Connaughton and J. D. Shephard, Laser textured superhydrophobic surfaces and their applications for homogeneous spot deposition, *Applied Surface Science*, 365 (2016) 153-159.

[45] Y. Cai, W. Chang, X. Luo, A. M. L. Sousa, K. H. A. Lau and Y. Qin, Superhydrophobic structures on 316L stainless steel surfaces machined by nanosecond pulsed laser, *Precision Engineering*, 52 (2018) 266-275.

[46] E. Paparazzo, XPS analysis of iron aluminum oxide systems, *Applied Surface Science*, 25 (1) (1986) 1-12.

[47] R. Jagdheesh, M. Diaz and J. L. Ocaña, Bio inspired self-cleaning ultrahydrophobic aluminium surface by laser processing, *RSC Advances*, 6 (77) (2016) 72933-72941.

[48] J. Cardoso, A. Garcia-Girón, J.-M. Romano, D. Huerta-Murillo, R. Jagdheesh, M. Walker, S. Dimov and J. L. Ocaña, Influence of ambient conditions on the evolution of wettability properties of an IR-, ns-laser textured aluminium alloy, *RSC Advances*, 7 (63) (2017) 39617-39627.

[49] J. van den Brand, S. Van Gils, P. C. J. Beentjes, H. Terryn and J. H. W. de Wit, Ageing of aluminium oxide surfaces and their subsequent reactivity towards bonding with organic functional groups, *Appl. Surf. Sci.*, 235 (4) (2004) 465-474.

[50] Z. Yang, X. Liu and Y. Tian, Insights into the wettability transition of nanosecond laser ablated surface under ambient air exposure, *Journal of Colloid and Interface Science*, 533 (2019) 268-277.

Changyoung Ryu is currently an Assistant Researcher in the School of Mechanical Engineering, Chung-Ang University, Seoul, South Korea. He received a master degree in mechanical engineering at Chung-Ang University in 2023. His research interests include micro-cooling devices, and laser processing.